Springer

Dear Author,

Here are the proofs of your article.

- You can submit your corrections **online**, via **e-mail** or by **fax**.
- For **online** submission please insert your corrections in the online correction form. Always indicate the line number to which the correction refers.
- You can also insert your corrections in the proof PDF and **email** the annotated PDF.
- For fax submission, please ensure that your corrections are clearly legible. Use a fine black pen and write the correction in the margin, not too close to the edge of the page.
- Remember to note the **journal title**, **article number**, and **your name** when sending your response via e-mail or fax.
- **Check** the metadata sheet to make sure that the header information, especially author names and the corresponding affiliations are correctly shown.
- **Check** the questions that may have arisen during copy editing and insert your answers/ corrections.
- **Check** that the text is complete and that all figures, tables and their legends are included. Also check the accuracy of special characters, equations, and electronic supplementary material if applicable. If necessary refer to the *Edited manuscript*.
- The publication of inaccurate data such as dosages and units can have serious consequences. Please take particular care that all such details are correct.
- Please **do not** make changes that involve only matters of style. We have generally introduced forms that follow the journal's style.
  Substantial changes in content, e.g., new results, corrected values, title and authorship are not allowed without the approval of the responsible editor. In such a case, please contact the Editorial Office and return his/her consent together with the proof.
- If we do not receive your corrections **within 48 hours**, we will send you a reminder.
- Your article will be published **Online First** approximately one week after receipt of your corrected proofs. This is the **official first publication** citable with the DOI. **Further changes are, therefore, not possible.**
- The **printed version** will follow in a forthcoming issue.

Please note

After online publication, subscribers (personal/institutional) to this journal will have access to the complete article via the DOI using the URL: http://dx.doi.org/[DOI].
If you would like to know when your article has been published online, take advantage of our free alert service. For registration and further information go to: http://www.link.springer.com.

Due to the electronic nature of the procedure, the manuscript and the original figures will only be returned to you on special request. When you return your corrections, please inform us if you would like to have these documents returned.

Metadata of the article that will be visualized in OnlineFirst

ArticleTitle	Fabrication of periodically micropatterned magnetite nanoparticles by laser-interference-controlled electrodeposition	
Article Sub-Title		
Article CopyRight	Springer Science+Business Media, LLC, part of Springer Nature (This will be the copyright line in the final PDF)	
Journal Name	Journal of Materials Science	
Corresponding Author	Family Name	**Wang**
	Particle	
	Given Name	**Zuobin**
	Suffix	
	Division	International Research Centre for Nano Handling and Manufacturing of China
	Organization	Changchun University of Science and Technology
	Address	Changchun, 130022, China
	Phone	+86 431 85582341
	Fax	
	Email	wangz@cust.edu.cn
	URL	
	ORCID	
Author	Family Name	**Wang**
	Particle	
	Given Name	**Lu**
	Suffix	
	Division	International Research Centre for Nano Handling and Manufacturing of China
	Organization	Changchun University of Science and Technology
	Address	Changchun, 130022, China
	Phone	
	Fax	
	Email	
	URL	
	ORCID	
Author	Family Name	**Dong**
	Particle	
	Given Name	**Litong**
	Suffix	
	Division	International Research Centre for Nano Handling and Manufacturing of China
	Organization	Changchun University of Science and Technology
	Address	Changchun, 130022, China
	Phone	

	Fax	
	Email	
	URL	
	ORCID	
Author	Family Name	**Li**
	Particle	
	Given Name	**Li**
	Suffix	
	Division	International Research Centre for Nano Handling and Manufacturing of China
	Organization	Changchun University of Science and Technology
	Address	Changchun, 130022, China
	Phone	
	Fax	
	Email	
	URL	
	ORCID	
Author	Family Name	**Weng**
	Particle	
	Given Name	**Zhankun**
	Suffix	
	Division	International Research Centre for Nano Handling and Manufacturing of China
	Organization	Changchun University of Science and Technology
	Address	Changchun, 130022, China
	Phone	
	Fax	
	Email	
	URL	
	ORCID	
Author	Family Name	**Xu**
	Particle	
	Given Name	**Hongmei**
	Suffix	
	Division	International Research Centre for Nano Handling and Manufacturing of China
	Organization	Changchun University of Science and Technology
	Address	Changchun, 130022, China
	Phone	
	Fax	
	Email	
	URL	
	ORCID	
Author	Family Name	**Yu**
	Particle	
	Given Name	**Miao**

	Suffix	
	Division	International Research Centre for Nano Handling and Manufacturing of China
	Organization	Changchun University of Science and Technology
	Address	Changchun, 130022, China
	Phone	
	Fax	
	Email	
	URL	
	ORCID	

Schedule	Received	18 September 2017
	Revised	
	Accepted	2 November 2017

Abstract

This paper introduces a laser-interference-controlled electrochemical deposition method for direct fabrication of periodically micropatterned magnetite (Fe_3O_4) nanoparticles (NPs). In this work, Fe_3O_4 NPs were controllably synthesized on the areas where the photoconductive electrode was exposed to the periodically patterned interferometric laser irradiation during the electrodeposition. Thus, the micropattern of Fe_3O_4 NPs was controlled by interferometric laser pattern, and the crystallization of the particles was controlled by laser interference intensity and electrochemical deposition conditions. The bottom-up electrochemical approach was combined with a top-down laser interference methodology. This maskless method allows for in situ fabrication of periodically patterned magnetite NPs on the microscale by electrodeposition under room temperature and atmospheric pressure conditions. In the experiment, Fe_3O_4 NPs with the mean grain size below 100 nm in the pattern of 5-μm line array were achieved within the deposition time of 100 s. The experiment results have shown that the proposed method is a one-step approach in fabricating large areas of periodically micropatterned magnetite NPs.

Footnote Information

_2D materials
_*ab initio* calculations
_additive manufacturing
_adhesion
_adsorption
_aerogels
_AFM
_alloys
_amorphous materials
_annealing
_antifouling materials
_atomic-layer deposition (ALD)
_atomistic modeling
_batteries
_batteries, lithium
_batteries, magnesium
_batteries, sodium
_BCC metals
_bio-inspired materials
_biomass conversion
_biomaterials
_biomechanics
_biomimetic
_black phosphorus
_blends
_brazing
_calcification
_capacitors
_carbon fiber
_carbon nanotube
_casting
_catalysts or catalysis
_cellular materials
_cellulose
_ceramics
_characterization methods
_chemical vapor deposition (CVD)
_CO_2 sequestration
_coatings
_colloids or bio-colloids
_composite materials
_computational materials science
_computer modeling
_computer simulation
_conducting polymers
_corrosion and oxidation
_corrosion protection
_crystal plasticity
_crystallization
_curing
_data analytics
_defects
_deformation
_deposition
_dielectrics
_diffraction, electron
_diffraction, neutron
_diffraction, X-ray (XRD)
_diffusion
_diodes
_dislocation dynamics
_dislocations
_drug delivery
_dye-sensitized solar cells (DSSCs)
_dysfunctional materials
_EBSD
_elastic properties
_electrical properties
_electrocatalysis
_electrochemistry
_electrode materials
_electron-beam melting
_electronic materials
_electronic properties
_electrospinning
_embrittlement
_energy harvesting
_epitactic or epitaxial growth
_fatigue
_FCC metals
_ferroelectrics
_FGMs
_fibers or fiber technology
_food colloids
_fracture
_fuel cells
_functional anisotropy
_functional materials
_gas-phase transport
_gelation
_geocomposites
_glass
_grain boundaries
_grain boundary engineering
_graphene
_graphitic carbon
_hardness
_HCP metals
_healing
_heat treatment
_hierarchical materials
_high entropy alloys
_high pressure torsion
_high throughput testing
_hot isostatic pressing
_hydrogels
_hydrogen storage or production
_hydrolysis
_II-VI compounds
_III-V compounds
_imaging
_In situ or operando
_infrared spectroscopy
_intercalation
_interfaces
_intermetallics
_ionomers
_kinetics
_laminates
_laser processing
_latticed effects
_layered materials
_light alloys
_light-emitting diodes
_liquid crystals
_lithography
_machining
_macro defects
_magnetic materials or properties
_magnetic ordering
_materials design
_materials for demanding environments
_materials for energy
_mechanical properties
_membranes
_mesoporous materials
_metal-insulator transition
_metal/organic frameworks (MOFs)
_metallic glasses
_metals
_metamaterials
_microanalysis
_microstructure
_minerals or mineralization
_molding
_molecular dynamics
_molecular simulation
_molecular-beam epitaxy (MBE)
_morphology
_multiferroics
_multilayers
_nanocomposites
_nanofunctionality
_nanoindentation
_nanolithography
_nanomaterials
_nanomedicines
_nanoporous materials
_natural materials
_NDT
_NMR
_nuclear materials
_nucleation
_omniphobic materials
_optical materials and properties
_organic electronics
_organic solar-cell materials
_permselective materials
_perovskite
_perovskite solar cell (PSCs)
_phase diagrams
_phase transformations
_phase-change materials (PCMs)
_phase-field modeling
_phosphors
_photocatalysis
_photonic materials
_photoreactive materials
_phototherapeutics
_photovoltaics (solar cells)
_piezoelectric materials
_plasma deposition
_plasmonic materials
_plating
_polymers
_porous materials
_powder technology
_pyroelectrics
_quasicrystals
_radiation damage
_radiation effects
_rapidly solidified materials
_redox flow batteries
_regenerative medicine
_resorbable materials
_responsive materials
_rheology
_sapphire/Al_2O_3
_scaffolds
_scanned-probe microcopy
_selective laser melting
_self-assembly
_self-healing materials
_SEM
_semiconductors
_sensing and sensors
_severe plastic deformation
_shape memory materials
_silicones
_singlet-exciton fission
_sintering
_small volume testing
_smart materials
_sodium-sulphur batteries
_soft interfaces
_soft matter
_sol-gel preparation
_solidification
_solvothermal/hydrothermal
_spectroscopy (XPS)
_spin glass
_spintronics
_sputter deposition
_STM
_superalloys
_supercapacitors
_superconductors
_superelasticity
_superhydrophobic
_surface treatments
_surfaces
_surfactants
_technical textiles
_TEM
_texture
_theranostics
_thermal barrier coatings
_thermal properties
_thermodynamics
_thermoelectrics
_thin-film or thick-film coatings
_TiO_2 rutile, anatase or brookite
_tissue engineering
_tomography
_topological insulators
_transparent conductors
_transport mechanisms
_tribology
_twinning
_TWIP steels
_two-photon adsorption
_UFG materials
_viscoelasticity
_viscosity
_water-splitting
_wear
_wood
_XPS
_zeolite

J Mater Sci

Ceramics

Fabrication of periodically micropatterned magnetite nanoparticles by laser-interference-controlled electrodeposition

Lu Wang[1], Litong Dong[1], Li Li[1], Zhankun Weng[1], Hongmei Xu[1], Miao Yu[1], and Zuobin Wang[1,*]

[1] *International Research Centre for Nano Handling and Manufacturing of China, Changchun University of Science and Technology, Changchun 130022, China*

Received: 18 September 2017
Accepted: 2 November 2017

ABSTRACT

This paper introduces a laser-interference-controlled electrochemical deposition method for direct fabrication of periodically micropatterned magnetite (Fe_3O_4) nanoparticles (NPs). In this work, Fe_3O_4 NPs were controllably synthesized on the areas where the photoconductive electrode was exposed to the periodically patterned interferometric laser irradiation during the electrodeposition. Thus, the micropattern of Fe_3O_4 NPs was controlled by interferometric laser pattern, and the crystallization of the particles was controlled by laser interference intensity and electrochemical deposition conditions. The bottom-up electrochemical approach was combined with a top-down laser interference methodology. This maskless method allows for in situ fabrication of periodically patterned magnetite NPs on the microscale by electrodeposition under room temperature and atmospheric pressure conditions. In the experiment, Fe_3O_4 NPs with the mean grain size below 100 nm in the pattern of 5-μm line array were achieved within the deposition time of 100 s. The experiment results have shown that the proposed method is a one-step approach in fabricating large areas of periodically micropatterned magnetite NPs. AQ1

Introduction

Micro- and nanopatterned magnetic nanoparticles (MNPs) are widely investigated recently due to the increasing demand of nanoelectronic devices, sensors [1, 2], systems for sorting and manipulating cells [3], and high-density data storage devices [4]. Nanoparticle-based structures specifically concern two-dimensional ordered arrays of MNPs on solid substrates which possess different properties of magnetic anisotropy [5, 6]. Such structures are particularly promising for the manufacturing of high-capacity bit-patterned media (BPM) [7], which can potentially extend the storage capacities of magnetic hard disk drives (HDDs) and replace present magnetic films. Conventional synthesis of patterned thin films of MNPs requires a high temperature of hundreds of degrees Celsius and high-vacuum sputtering

Address correspondence to E-mail: wangz@cust.edu.cn

DOI 10.1007/s10853-017-1788-9

Journal : 10853 - Large 10853 | Dispatch : 6-11-2017 | Pages : 11
Article No. : 1788 | ☐ LE | ☐ TYPESET
MS Code : JMSC-D-17-05919 | ☑ CP | ☑ DISK

process with specialized equipment [8, 9]. Therefore, the development of economical synthesis methods for the fabrication of MNPs with a controllable pattern, period and crystallization is required [10].

Currently, iron oxides such as magnetite (Fe_3O_4) can be obtained by cathodic or anodic electrochemical synthesis methods [11–14]. Martinez et al. [11] reported that iron oxide–oxyhydroxide layers in different phases were able to be produced by the control of applied voltages and electrolyte compositions. Meng et al. [12] reported the fabrication of hematite (α-Fe_2O_3) nanoparticles (NPs) on ITO films by electrodeposition. The electrochemical deposition of Fe_3O_4 micro–nanoparticles on carbon nanofiber buckypapers was reported [13]. Cathodic electrodeposition of Fe_3O_4 thin films by galvanostatic deposition at elevated temperatures was also reported [14]. It can be seen from the reported approaches that the NPs are fabricated with unpatterned electrodes in the electrochemical deposition processes. Therefore, patterned distributions of particles cannot be obtained by the reported methods, and there is the need to develop methods for direct fabrication of patterned particles.

Normally, lithography-assisted assembly is the main methodology for organizing MNPs into micro-/nanostructured patterns on a substrate. Stamp-assisted structuration method is most widely used for patterning MNPs on surfaces by microcontact printing (μCP). A self-assembled monolayer (SAM) was fabricated as a template, and then the MNPs were attached to the structured surfaces [15–18]. Also, Cavallini et al. [19] reported the method of microinjection molding in capillaries to pattern Fe_3O_4 NPs in micrometric stripes and dots on mica. Electron beam lithography (EBL) and photolithography are mostly used in the lithography-assisted structuration method to fabricate physical templates that can be used to structure the MNPs. The topographically structured surfaces physically guide the assembly of MNPs to specific areas [20–22]. Recently, biomimetic templates are used for the synthesis and assembly of MNPs. Patterning of magnetite NPs onto gold substrates by biomineralization and biotemplate has been previously reported [23–26]. Although different methods for the fabrication of ordered MNPs have been developed, the patterned templates obtained by relatively complex traditional lithography steps are usually required. The optically induced electrochemical deposition (OED) method [27–29], previously developed by Li et al., used programmable light patterns to produce controlled and localized electric fields in a photosensitive microfluidic chip, for fabricating metal thin films in nanodevices.

In this study, we combined the electrodeposition with the OED method and presented a laser interference controlled electrochemical deposition (LIED) method to achieve direct and high-efficient fabrication of periodically micropatterned Fe_3O_4 NPs on large areas. Laser interference irradiation was used in the LIED process to generate periodic microstructures over large areas with high-fidelity and minimal substrate treatments [30–33]. Fe_3O_4 NPs in a periodical pattern of 5-μm line arrays were directly fabricated by LIED over an area of 1 cm^2 within 100-s deposition time, and the mean grain size of the NPs was below 100 nm. The process was performed in one-step at room temperature and atmospheric pressure conditions, while requiring no templates and complex techniques.

The LIED method has good controllability for the fabrication of patterned MNPs. During electrodeposition, the synthesis of MNPs occurs selectively on the areas where the photoconductive cathode is exposed to the interferometric laser irradiation in the electrolyte. Therefore, the micropattern period along with the pattern of the MNPs is controlled by the interferometric laser pattern. The nucleation and growth of Fe_3O_4 NPs are controlled by the laser interference intensity and electrochemical deposition conditions of the applied potential and deposition time.

Periodically micropatterned Fe_3O_4 NPs fabricated by LIED method on hydrogenated amorphous silicon (α-Si:H) were investigated for the first time to understand the patterning mechanism of the laser interference controlled process and the electrodeposition reaction. Also, the effects of interference intensity, electrodeposition potential and time on the grain size, crystallization, and morphology of Fe_3O_4 were subsequently studied. The optimization of conditions in electrosynthesis was also carried out.

Methods

Experiment

Preparation of electrolyte

The electrolyte used in each experiment was a mixture of 4 mM ferrous chlorides ($FeCl_2{\cdot}4H_2O$, Xilong

Journal : 10853 - Large 10853 | Dispatch : 6-11-2017 | Pages : 11
Article No. : 1788 | LE | TYPESET
MS Code : JMSC-D-17-05919 | CP | DISK

AQ2 Chemical) and 8 mM ferric chlorides ($FeCl_3 \cdot 6H_2O$, Tianjin Kaitong Chemical Reagent) containing Fe^{2+}/Fe^{3+} ions with a molar ratio of 1:2, based on the co-precipitation method for the preparation of bare Fe_3O_4 NPs [34]. The electrolyte was put in a 150 mL rectangular quartz beaker. All electrolytes were prepared from analytical grade reagents without further purification, and deionized water was from the Millipore water purification system. The electrolyte was kept at room temperature during the entire electrodeposition process.

Electrode fabrication

The photoconductive electrode consists of an ITO glass substrate (square resistance is 8 Ω) with an α-Si:H layer deposited on the substrate surface by a plasma-enhanced chemical vapor deposition (PECVD) process. During the PECVD, one part of the ITO glass was covered with a mask, leaving a non-deposited area used as a bottom conductive electrode. Then, a copper conductive tape was connected to the exposed bottom ITO electrode so as to enhance the conductivity when applying a DC current to the electrode, as shown in the enlarged image of Fig. 1a. Specifically, the thickness of the α-Si:H layer was 100 nm. The counter electrode was an iron plate, and the reference electrode was a saturated calomel electrode (SCE). Prior to the electrodeposition, the three-electrode setup was immersed in the electrolyte, and the photoconductive electrode was placed on the outermost side. The uncoated side was directed toward the beaker wall with the α-Si:H film oriented toward the inside of the beaker. The immersion depth of the electrodes was consistent to ensure that the area deposited in each experiment was about 1 cm^2, and the position of the electrodes was fixed.

Experiment setup

The laser interference irradiation process was carried out by exposing the photoconductive electrode surface to a continuous wave Nd: YAG laser (CNI MSL-457, $\lambda = 457$ nm, maximum power = 100 mW) in a two-beam interference system. The laser power was measured with the Laser Power and Energy Meter (Thorlabs PM200). The schematic diagram of the interference system setup is shown in Fig. 1a. W is the half-wave plate, and P is the polarization prism. M is the mirror, and BS is the beam splitter. In the experiment, the two incident beams followed a symmetrical configuration with the azimuthal angles of $\varphi_1 = 0°$ and $\varphi_2 = 180°$ and the same incident angle of 2.6°. The polarization mode of TE–TE was employed. It was assumed that the initial phases were zero and the amplitudes of the two beams were identical. The interference system was mounted on the outside of the beaker to ensure the homogeneous illumination during deposition. The laser beams were expanded so that they illuminated an area of 1 cm^2. The beams were reflected off the mirrors and passed through the beaker, electrolyte and ITO substrate. Then they were intersected and interfered on the back of the α-Si:H film. An electrochemical workstation (Model CHI660D, Shanghai Chenhua) was interfaced to a personal computer for collecting data. The measurement method of chronopotentiometry (CP) was used for the electrochemical deposition. The cathode of the electrochemical workstation was connected to the ITO layer of the photoconductive substrate via the conductive copper tape. The complete LIED system is shown in Fig. 1a.

Fabrication of Fe_3O_4 NPs by LIED method

When a DC current was applied between the cathode and the metallic anode, concurrently, laser interference irradiated on the photoconductive substrate, and the electrochemical deposition was carried out with the different time periods from 0 to 800 s. Finally, the deposited NPs were rinsed with DI water and dried with nitrogen. A large area of Fe_3O_4 NPs in the pattern of 5-μm line arrays was obtained on the α-Si:H surface as shown in Fig. 1b. The grain size distribution of particles has a good agreement with the distribution of the interferometric laser intensity, as shown in Fig. 1c. The details will be discussed in "Laser interference irradiation-dependent grain size distribution" section.

Characterization

A scanning electron microscope (SEM) was used to examine the morphologies and grain distributions. All deposited samples were imaged by a high-resolution SEM (FEI QUANT-250 FEG, at the 5 kV accelerated voltage). X-ray photoelectron spectroscopy (XPS) was used to identify the element

Journal : 10853 - Large 10853 | Dispatch : 6-11-2017 | Pages : 11
Article No. : 1788 | LE | TYPESET
MS Code : JMSC-D-17-05919 | CP | DISK

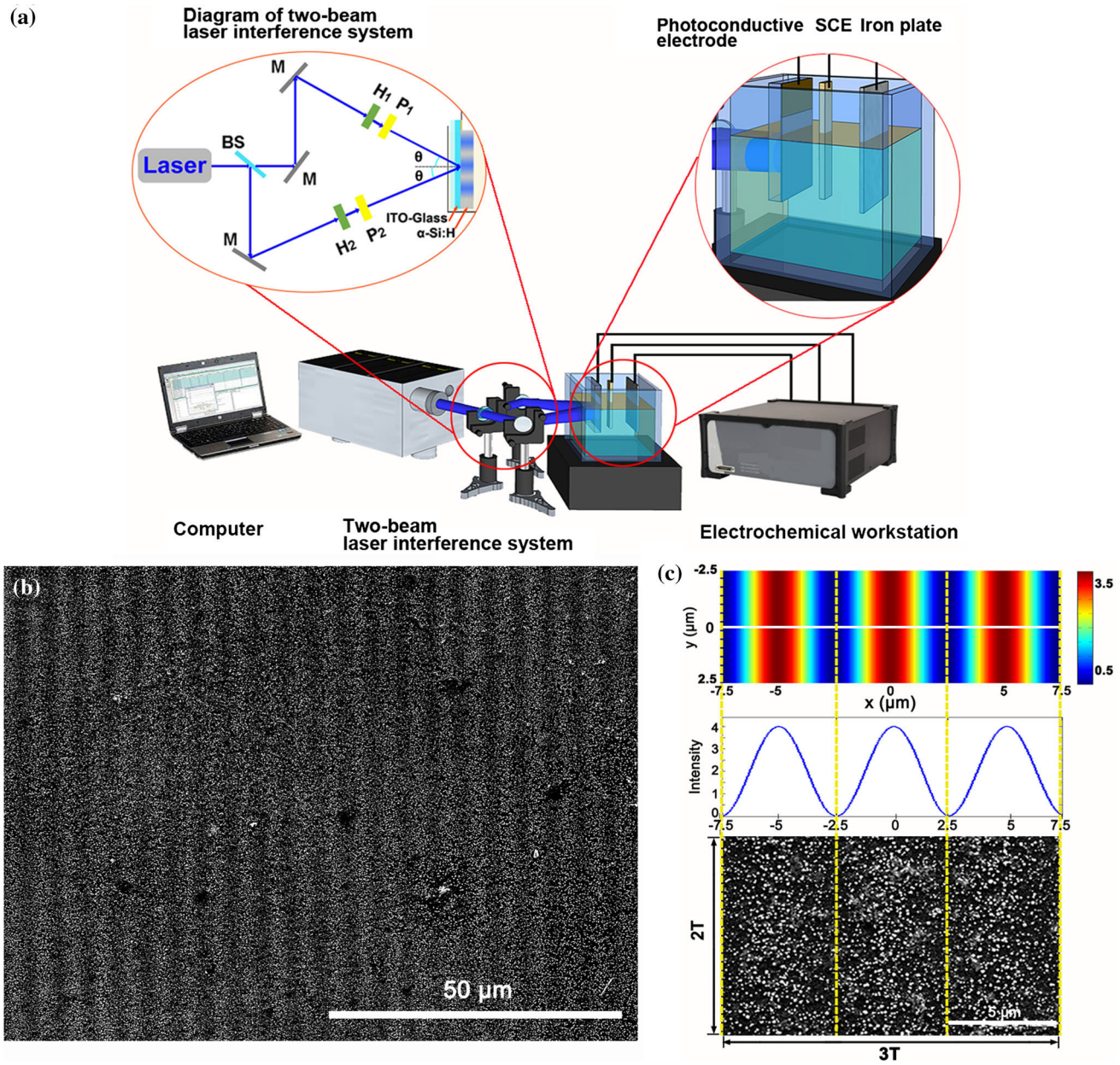

Figure 1 **a** LIED experimental system and diagram of two-beam laser interference system. **b** Large area of Fe_3O_4 NPs fabricated on the α-Si:H surface. **c** 2D interference simulation result for two-beam laser interference pattern ($\lambda = 457$ nm, $\theta = 2.6°$) and the corresponding laser intensity curve along the line in the simulation, and the consistent distribution of Fe_3O_4 NPs with an area of $2T \times 3T$, where T is the period.

constituents of the deposits. The crystal phase of samples was characterized by XPS (ESCALAB 250).

Figure 2 shows the XPS spectra of the Fe_3O_4 NPs fabricated on the α-Si:H surface with the current density of 1.0 mA cm^{-2}, deposition time of 100 s and irradiated interferometric laser power density of 1.5 mW cm^{-2}. The peaks of the C 1*s*, O 2*p*, Fe 3*p*, and Fe 2*p* are included in the NPs, as shown in Fig. 2a. Fe_3O_4 is alternatively expressed as $FeO{\cdot}Fe_2O_3$. From the spectra in Fig. 2b, the double peak positions of Fe $2p_{3/2}$ and Fe $2p_{1/2}$ are 710.88 and 724.48 eV, respectively, which are in agreement with the standard peak positions of Fe^{3+} and Fe^{2+} in the stoichiometric Fe_3O_4 [11, 35]. The double peaks are broadened, corresponding to the contributions of Fe^{2+} ($2p_{3/2}$) and Fe^{2+} ($2p_{1/2}$) peaks. This situation confirms that the NPs are Fe_3O_4 rather than γ-Fe_2O_3 [36, 37].

Journal : 10853 - Large 10853 | Dispatch : 6-11-2017 | Pages : 11
Article No. : 1788 | LE | TYPESET
MS Code : JMSC-D-17-05919 | CP | DISK

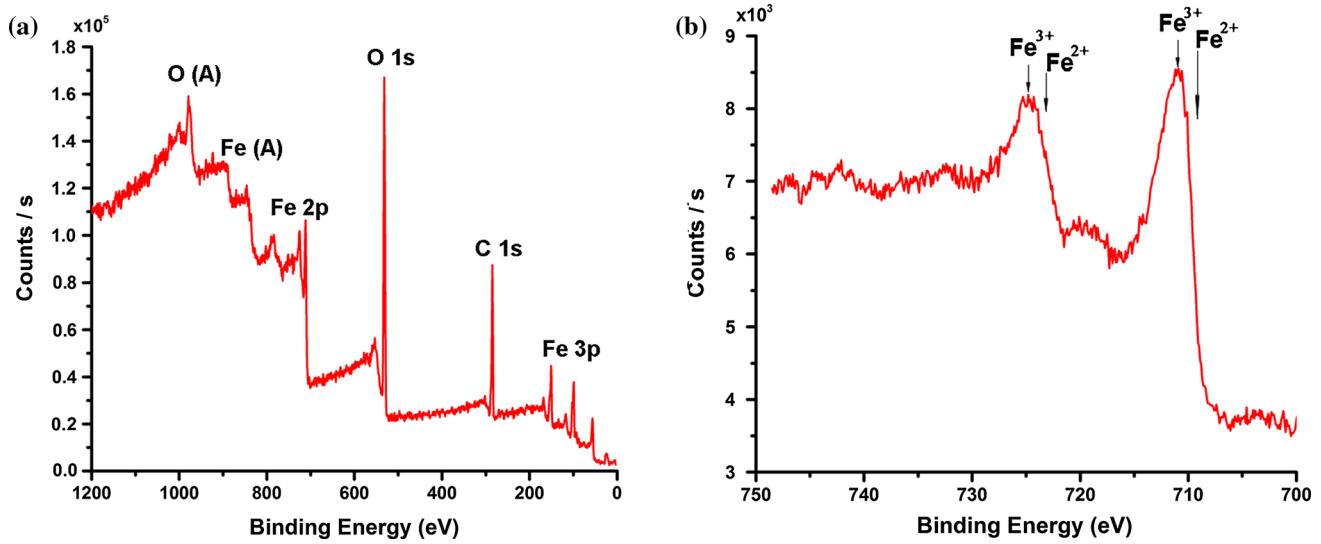

Figure 2 **a** XPS spectra of the constituent elements for the Fe_3O_4 NPs fabricated on the α-Si:H surface with the current density of 1.0 mA cm^{-2}, deposition time of 100 s and irradiated interferometric laser power density of 1.5 mW cm^{-2}. **b** Detailed peaks of Fe $2p_{1/2}$ and Fe $2p_{3/2}$.

Patterning mechanism by LIED

The laser interference irradiation on the photoconductive cathode and an applied DC current concurrently perform the LIED patterning process. The photoconductivity of the irradiated α-Si:H can increase from 10^{-10} S m^{-1} to approximately 10^{-3} S m^{-1}, resulting from the photoexcitation of electron–hole pairs. When the interferometric laser intensity reaches to a certain threshold, the incident interferometric laser pattern on the photoconductive substrate generates localized micropatterns of high conductivity, leading to the creation of a patterned virtual photo-cathode or virtual electrode (VE). In this way, the patterned laser irradiation controls the electrodeposition reaction as an optical switch. As shown in Fig. 3a, the interferometric laser pattern irradiated onto the α-Si:H substrate of the cathode forms a patterned VE and guides the electron transfer with the pattern. Under an applied galvanostatic condition, a higher electrical potential could be dropped on the VE/electrolyte area than the non-irradiated interface. Due to the effects of electrophoretic force and Brownian motion, the mass transfers of ferrous irons and ferric irons are from the electrolyte solution to the reaction zone.

Then the adsorbed ferrous irons, ferric irons and hydroxyl ions generated from the reaction in Eq. (1), allow for the electrochemical synthesis of Fe_3O_4 in the electric double layer (EDL) [38, 39] close to the VE, as

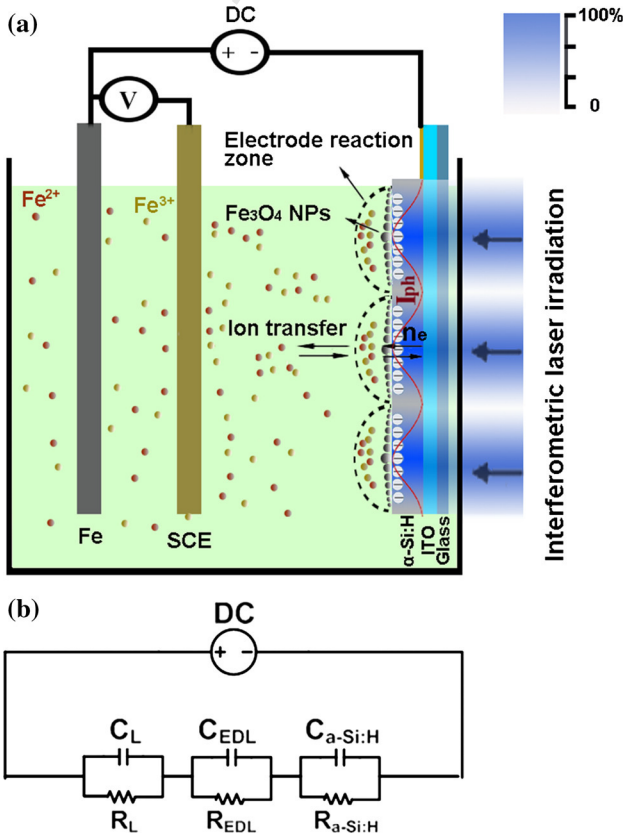

Figure 3 **a** Mechanism of fabricating patterned Fe_3O_4 NPs by LIED. The cathode consists of the ITO glass substrate and α-Si:H film on the surface. **b** Equivalent circuit model of the LIED system, which consists of the α-Si:H film, the iron ion electrolyte and the VE/electrolyte interface.

Journal : 10853 - Large 10853 | Dispatch : 6-11-2017 | Pages : 11
Article No. : 1788 | LE | TYPESET
MS Code : JMSC-D-17-05919 | CP | DISK

shown in Eq. (2). At the VE, the evolution of hydrogen gas is accompanied by the formation of OH^- ions, which will lead to an increase in the local pH at the electrode surface.

The cathode reactions in the reaction zone can be expressed as

$$2H_2O + 2e^- \rightarrow H_2 + 2OH^- \quad (1)$$

$$Fe^{2+} + 2Fe^{3+} + 8OH^- \rightarrow Fe_3O_4 + 4H_2O. \quad (2)$$

In the LIED system, the EDL at the interface between the VE and the electrolyte, plays a pivotal role for the overall reaction, because it provides the voltage potential and environment for the final product [40, 41]. Figure 3b shows a simplified equivalent circuit model of the LIED system, where C_a and R_a denote the capacitance and resistance of the α-Si:H layer, C_L and R_L denote the capacitance and resistance of the electrolyte, and C_{EDL} and R_{EDL} indicate the equivalent capacitance and resistance of the EDL between the VE and electrolyte interface.

Magnetite molecules nucleated on the illuminated surface and aggregated into NPs with the same pattern as the projected interferometric laser. Thus, the period of the patterned NPs can be controlled directly, and the grain size distribution is consistent with the interference intensity distribution.

Results and discussion

Grain size distribution

According to the Faraday's law of electrolysis, when a DC current flows through the electrolyte, the amount of substance nFe_3O_4 generated by the chemical reaction on an electrode (e.g., the VE/electrolyte interface) in a deposition process can be calculated by

$$n_{Fe_3O_4} = \frac{Q}{zF} \quad (3)$$

$$Q = I_{ph}t \quad (4)$$

where Q is the amount of electrons received, z is the valence of Fe_3O_4 molecules and F is the Faraday constant. In Eq. (4), I_{ph} denotes the photocurrent generated in the hydrogenated amorphous silicon, and t denotes the deposition time. When the illumination and electron–hole generation are in a steady-state throughout the α-Si:H material, and there is only the electron contribution to the photocurrent, the photoconductivity is written as [42]

$$\Delta\sigma_{ph} = \Phi\alpha\eta e\mu_{n0}\tau \quad (5)$$

where $\Delta\sigma_{ph}$ is the photoconductivity, Φ is the incident luminous flux per unit area, α is the absorption coefficient, η is the quantum efficiency for the electron generation, μ_{n0} is the drift mobility of the electron, and τ is the response time of photoconductivity. When the DC current is applied, the I_{ph} can be expressed as

$$I_{ph} = U\Delta\sigma_{ph}A/d \quad (6)$$

where U denotes the potential of the EDL, A is the pattern area, and d denotes the thickness of the α-Si:H film.

$$m_{Fe_3O_4} = V_{Fe_3O_4}\rho = Ar_{Fe_3O_4}\rho = n_{Fe_3O_4}N_{Fe_3O_4} \quad (7)$$

In Eq. (7), $r_{Fe_3O_4}$ is the grain size of Fe_3O_4 NPs. $N_{Fe_3O_4}$, $m_{Fe_3O_4}$, $V_{Fe_3O_4}$ and ρ are the molar mass, mass, volume, and density of Fe_3O_4, respectively.

Considering Eqs. (1–7), when the material of α-Si:H is not changed, $\alpha\eta e\mu_{n0}\tau N_{Fe3O4}/\rho zdF$ is a constant, and then the dependence of the grain size of the NPs can be expressed as

$$r_{Fe_3O_4} \propto U\Phi t \quad (8)$$

in which the grain size of the NPs is proportional to the applied potential, deposition time and laser intensity.

Laser interference irradiation-dependent grain size distribution

In this work, the intensity distribution of the two-beam interference pattern was obtained by theoretical analysis and computer simulation as shown in Fig. 1c. The details of the simulations can be found in our previous work [30–33]. The corresponding distribution of Fe_3O_4 NPs shows that the largest NPs are mainly concentrated in the interference maxima areas and the smallest ones in the interference minimum areas. The grain sizes are distributed in a gradient way. When the incident angles and intensities of laser beams are set to the same values, the period of two-beam interference pattern is $d = \lambda/2\sin(\theta)$. Therefore, the period of the patterned NPs can be controlled by changing the incident wavelength λ and the incident angle θ.

Journal : 10853 - Large 10853 Dispatch : 6-11-2017 Pages : 11
Article No. : 1788 LE TYPESET
MS Code : JMSC-D-17-05919 CP DISK

It can be found from Eq. (8) that when the potential and deposition time in the LIED process are constant, the grain size distribution of the NPs is determined by interferometric laser intensity. Figure 1c shows that the theoretical analysis matches well with the experimental results. The grain size distribution of NPs is also strongly dependent on the contrast of interferometric laser pattern which can be modulated by the parameters of incident beams. When the laser intensity is lower than the conducting threshold, the hydrogenated amorphous silicon film is not conductive, and when it is beyond the saturation threshold, the contrast of the pattern is decreased. Therefore, an optimal power density of 1.5 mW cm^{-2} for the irradiated interferometric laser was chosen for each experiment.

Relationship between the grain size and applied potential

The applied potential is a key factor in the deposition of patterned Fe_3O_4 NPs, and it greatly influences the properties of EDL. As shown in Fig. 4, the influence of the potential on the deposition of NPs was investigated.

The LIEDs were carried out at constant current densities of 0.5, 0.8, 1.0, 1.5, and 2.0 mA cm^{-2}, respectively. During the deposition time of 100 s, the potentials between the α-Si:H substrate cathode and the SEC in the electrolyte vs the deposition time were recorded, as shown in Fig. 4a. Based on the curve, an initial charging process of the negative potential was recorded with the time of the current applied to the cathode at the beginning, due to the large capacitance of the EDL.

In the experiments, the potential is proportional to the applied current density. The SEM micrograph of bare α-Si:H substrate before deposition is shown in Fig. 4b. Figure 4c–g shows the morphologies of five representative samples. With an applied potential between 0 and − 1.0 V, there are not patterned NPs observed, as shown in Fig. 4c. Figure 4d–f shows the microstructures of deposited Fe_3O_4 with different potentials. The particle size increases with the decrease in the applied negative potential. This can be attributed to that the applied higher current facilitates the higher reaction efficiency of Fe_3O_4 NPs.

When the applied negative potential is lower than − 3.0 V, the destruction of the hydrogenated amorphous silicon that results from the poor adherence of the film to the substrate can be observed (Fig. 4g). Therefore, the cathode current density for the crystallization of micropatterned Fe_3O_4 NPs is believed to be in a narrow range between 0.8 and 1.8 mA cm^{-2} for the electrodeposition. Correspondingly, the deposition potential window is between − 1.6 and − 3.0 V.

Relationship between the grain size and deposition time

Figure 5a–e shows the SEM images of the Fe_3O_4 particles in different deposition periods, with a fixed current density of 1.0 mA cm^{-2}. The grain size of the deposited particles increases with the deposition time of (a) 50 s, (b) 100 s, (c) 200 s, (d) 400 s, and (e) 800 s, respectively. The aggregation of Fe_3O_4 particles can be found due to the continued growth of particles and results in the formation of large Fe_3O_4 polycrystalline clusters once the α-Si:H substrate is completely covered with Fe_3O_4. Prolonging deposition duration leads to thick and dense magnetite deposits, as shown in Fig. 5e. The average grain size of particles in the micropattern is linearly proportional to the deposition time, as shown in Fig. 5f.

Grain size analysis in one $T \times T$ area

In this work, Fe_3O_4 NPs with different morphologies including tetragonal and irregular polyhedrons were synthesized. In particular, tetrahedral Fe_3O_4 NPs are featured with the regular shape, smooth surface and good crystallization [43]. Figure 6a shows the SEM images of Fe_3O_4 NPs fabricated on the α-Si:H substrate by LIED method in one $T \times T$ area. The applied current density is 1.0 mA cm^{-2} with the deposition time of 100 s. Software Image J and software Origin were used to calculate the grain sizes of NPs. The longest axis of NPs with the good contrast between the crystallization area and the substrate in SEM images was measured using Image J, and the results were collected and plotted by Origin software, as shown in Fig. 6b. The calculated mean size of NPs was 66.8 nm. It can be seen that the LIED method is able to fabricate patterned NPs with a near Gaussian distribution of grain sizes, giving an integrated method to control MNP morphology and localization on the surfaces with interference patterns.

Clearly, the LIED method could be improved by reducing the period of laser interference pattern to

Journal : 10853 - Large 10853 Dispatch : 6-11-2017 Pages : 11
Article No. : 1788 LE TYPESET
MS Code : JMSC-D-17-05919 CP DISK

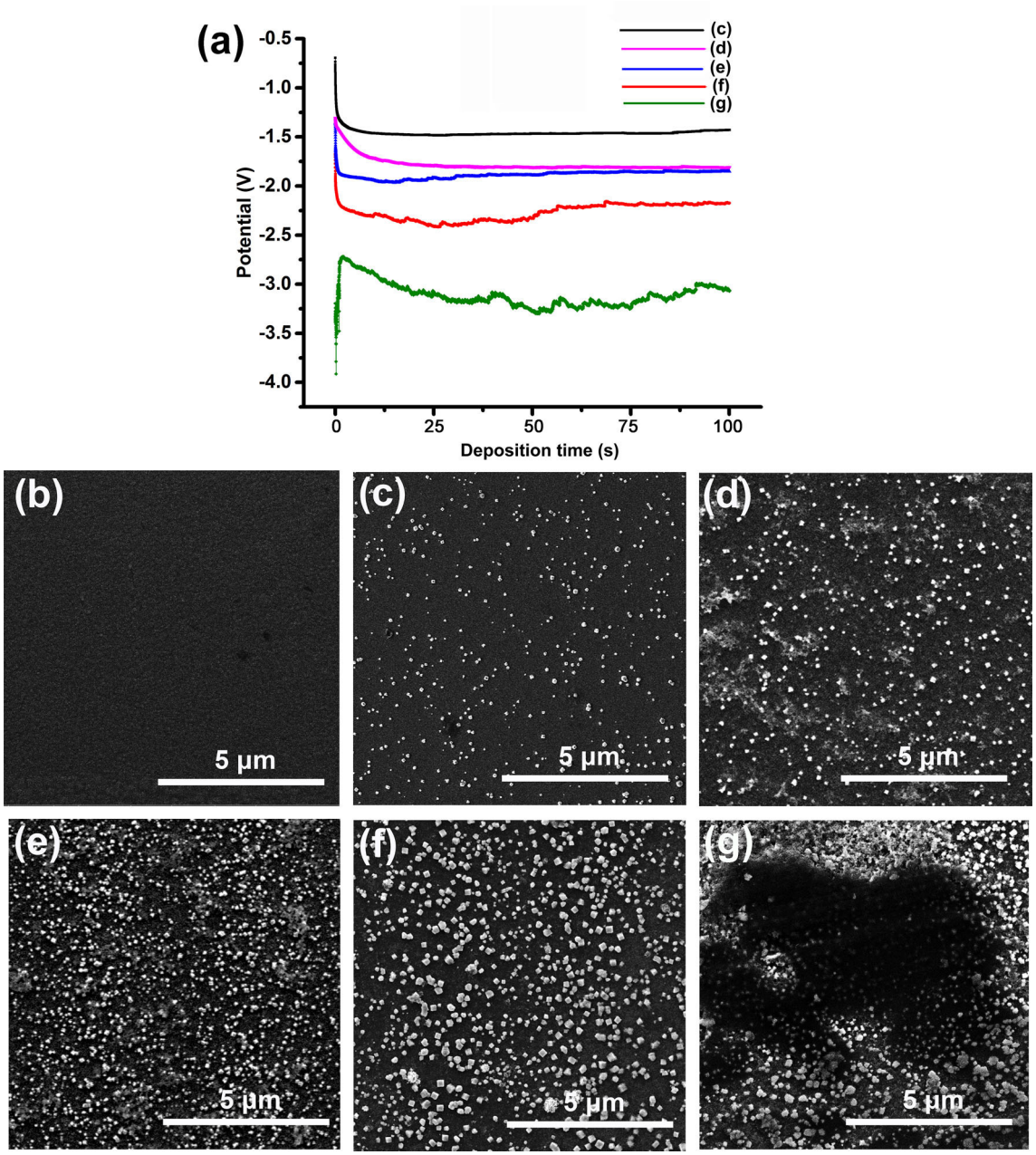

Figure 4 **a** Curves of potential versus time from the CP measurement under the applied current densities from (*c*–*g*): (*c*) 0.5 mA cm^{-2}, (*d*) 0.8 mA cm^{-2}, (*e*) 1.0 mA cm^{-2}, (*f*) 1.5 mA cm^{-2} and (*g*) 2.0 mA cm^{-2}, respectively. **b** SEM micrograph of bare α-Si:H substrate before deposition. **c**–**g** SEM micrographs of Fe_3O_4 NPs with an area of $2T \times 2T$.

nanoscales. The minimum period of the interference pattern is the half-wavelength of incident light. Laser interference can make different patterns, e.g., dot arrays with nanoscale precision can be generated by two identical exposures. Besides fabricating micropatterned Fe_3O_4 NPs, the LIED method is able to fabricate other MNPs or metal NPs such as copper, gold, CoPt and FePt with corresponding electrolytes.

Conclusions

In this work, a large area of periodically micropatterned Fe_3O_4 NPs was fabricated by LIED method. Fe_3O_4 NPs in a periodical pattern of 5-μm line arrays were synthesized on the hydrogenated amorphous silicon photoconductive cathode during the electrodeposition controlled by two-beam laser interference irradiation. The pattern of Fe_3O_4 NPs was

Journal : 10853 - Large 10853 | Dispatch : 6-11-2017 | Pages : 11
Article No. : 1788 | LE | TYPESET
MS Code : JMSC-D-17-05919 | CP | DISK

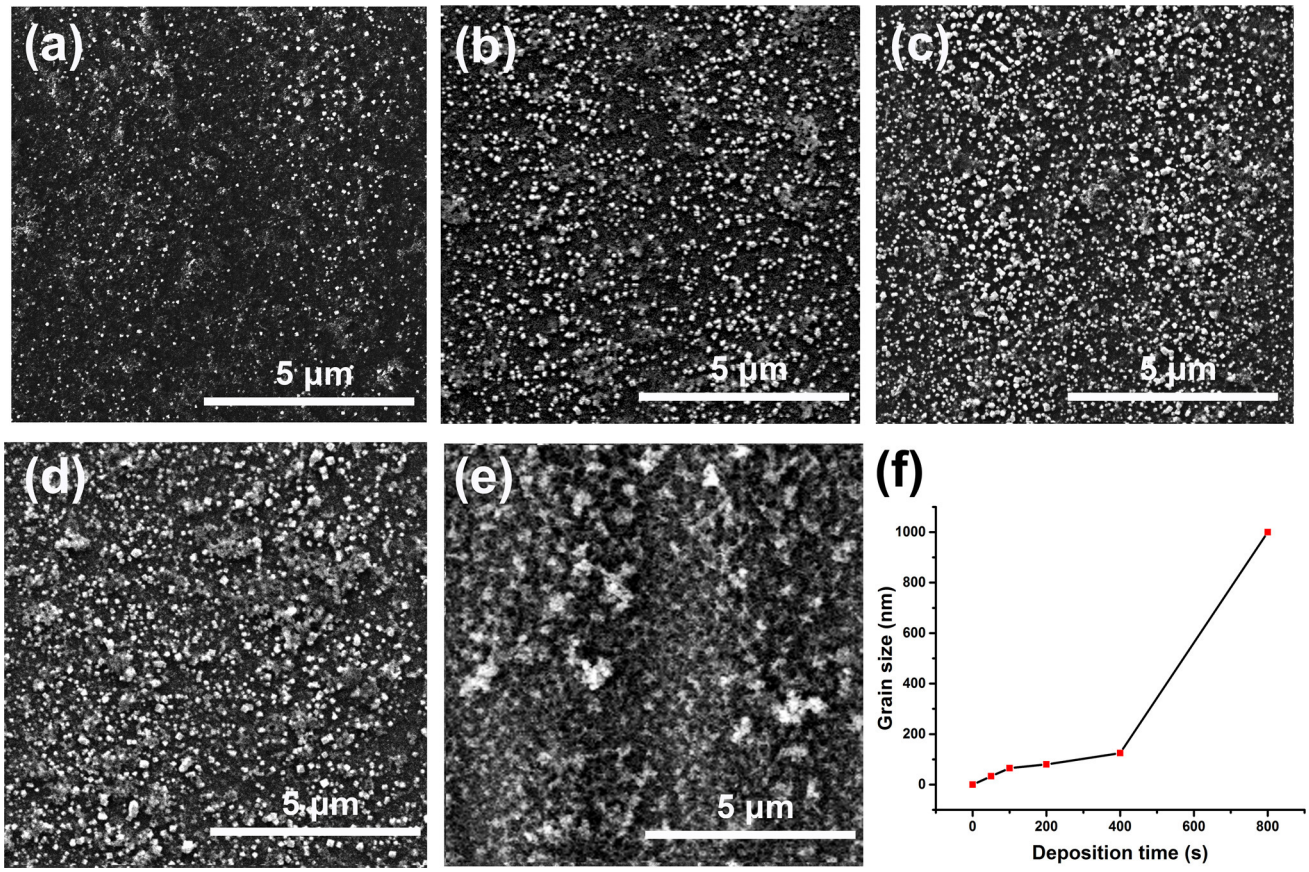

Figure 5 Morphologies of Fe_3O_4 particles at different deposition periods: **a** 50 s, **b** 100 s, **c** 200 s, **d** 400 s and **e** 800 s, respectively, with the current density of 1.0 mA cm^{-2} and the area of $2T \times 2T$. **f** Average grain sizes of Fe_3O_4 particles as a function of deposition time in (**a**–**e**).

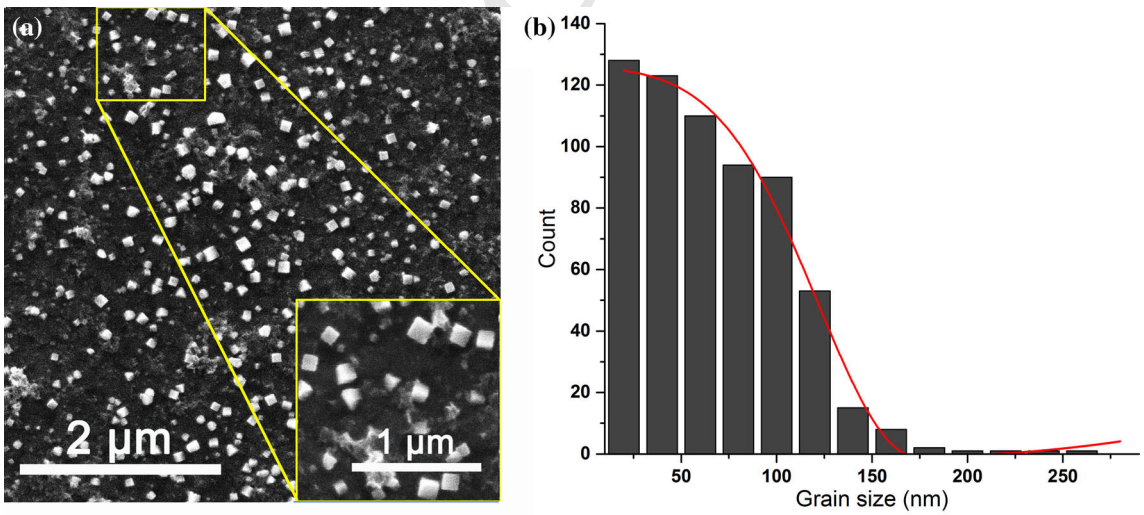

Figure 6 **a** SEM images of patterned Fe_3O_4 NPs fabricated by LIED method in an area of $T \times T$. **b** Counts of different grain sizes of Fe_3O_4 NPs within the area of (**a**).

Journal : 10853 - Large 10853 | Dispatch : 6-11-2017 | Pages : 11
Article No. : 1788 | ☐ LE | ☐ TYPESET
MS Code : JMSC-D-17-05919 | ☑ CP | ☑ DISK

controlled by the interferometric laser pattern, and the nucleation and growth of Fe_3O_4 NPs were controlled by the laser interference intensity and electrochemical deposition conditions of the applied potential and deposition time. The experimental results have shown that periodical micropatterns and grain sizes of Fe_3O_4 NPs can be fabricated in a controllable way with the LIED method. This work provides a one-step approach in fabricating a large area of periodically micropatterned MNPs for different potential applications.

Acknowledgements

This work was supported by the "111" Project of China (D17017), National Key Basic Research Program of China (973 Program No. 2012CB326406), EU FP7 (BioRA No. 612641), China-EU H2020 (FabSurfWAR Nos. 2016YFE0112100 and 644971), EU H2020 (MNR4SCell No. 734174), National Natural Science Foundation Program of China (Nos. 61176002, 11103047 and 11504030), and Jilin Provincial Science and Technology Program (Nos. 20160520101JH, 20160101318JC and 20160623002TC).

Compliance with ethical standards

Conflict of interest The authors declare that they have no conflict of interest.

References

[1] Lisa J, Daniel K, Rahel K, Johannes R, Piriya T et al (2015) Recent developments of magnetoresistive sensors for industrial applications. Sensors 15:28665–28689

AQ3 [2] Corteleón H, Nabaei V, Manzin A, Fletcher J, Krzysteczko P et al (2014) Anisotropic magnetoresistance state space of permalloy nanowires with domain wall pinning geometry. Scientific Reports 4:6045

[3] Cuong LV, Nghia NX, Thang PD (2015) Sorting and trapping human cells using a matrix of square micro-magnets. Mater Trans 56:1431–1433

[4] Lister SJ, Thomson T, Kohlbrecher J, Takano K, Venkataramana V et al (2010) Size-dependent reversal of grains in perpendicular magnetic recording media measured by small-angle polarized neutron scattering. Appl Phys Lett 97:011301

[5] Pauly M, Pichon BP, Panissod P, Fleutot S, Rodriguez P et al (2012) Size dependent dipolar interactions in iron oxide nanoparticle monolayer and multilayer Langmuir–Blodgett films. J Mater Chem 22:6343–6350

[6] Bedanta S, Kleemann W (2008) Supermagnetism. J Phys D Appl Phys 42:013001

[7] Hellwig O, Berger A, Thomson T, Dobisz E, Bandic ZZ et al (2007) Separating dipolar broadening from the intrinsic switching field distribution in perpendicular patterned media. Appl Phys Lett 90:R199

[8] Yu LN, Lu LY, Xu ZD, Xu XG, Miao J et al (2012) Enhanced L 1 0 phase transition in CoPt/Ag core/shell nanoparticles. Mater Lett 86:142–145

[9] Mosendz O, Pisana S, Reiner JW, Stipe B, Weller D (2012) Ultra-high coercivity small-grain FePt media for thermally assisted recording (invited). J Appl Phys 111:10

[10] Brown S (2012) Developments in data storage: materials perspective. Platin Met Rev 56:262–266

[11] Martinez L, Leinen D, Martín F, Gabas M, Ramos-Barrado JR et al (2007) Electrochemical growth of diverse iron oxide (Fe_3O_4, α-FeOOH, and γ-FeOOH) thin films by electrodeposition potential tuning. J Electrochem Soc 154:D126–D133

[12] Meng Q, Wang Z, Chai X, Weng Z, Ding R et al (2016) Fabrication of hematite (α-Fe_2O_3) nanoparticles using electrochemical deposition. Appl Surf Sci 368:303–308

[13] Li D, Zhou X, Xu Z, Man J, Yuan B et al (2015) Electrodeposition of micro-nano size Fe_3O_4 crystals anchored on flexible buckypaper. J Solid State Electrochem 19:3053–3058

[14] Duan H, Chen X, Li B, Liang J (2010) Growth morphology study of cathodically electrodeposited Fe_3O_4 thin films at elevated temperatures. Mater Res Bull 45:1696–1702

[15] Jie Y, Niskala JR, Johnston-Peck AC, Krommenhoek PJ, Tracy JB et al (2012) Laterally patterned magnetic nanoparticles. J Mater Chem 22:1962–1968

[16] Palacin S, Hidber PC, Bourgoin J, Miramond C, Fermon C et al (1996) Patterning with magnetic materials at the micron scale. Chem Mater 8:1316–1325

[17] An L, Li W, Nie Y, Xie B, Li Z et al (2005) Patterned magnetic rings fabricated by dewetting of polymer-coated magnetite nanoparticles solution. J Colloid Interface Sci 288:503–507

[18] Oktay Y, Tian G, Sachin K, Reinhoudt DN, Blank DH et al (2010) Monolayer-directed assembly and magnetic properties of FePt nanoparticles on patterned aluminum oxide. Int J Mol Sci 11:1162–1179

[19] Cavallini M, Bystrenova E, Timko M, Koneracka M, Zavisova V et al (2008) Multiple-length-scale patterning of magnetic nanoparticles by stamp assisted deposition. J Phys Condens Matter Inst Phys J 20:204144

Journal : 10853 - Large 10853 | Dispatch : 6-11-2017 | Pages : 11
Article No. : 1788 | ☐ LE | ☐ TYPESET
MS Code : JMSC-D-17-05919 | ☑ CP | ☑ DISK

[20] Chen G, Bodnarchuk MI, Kovalenko MV, Springholz G, Heiss W et al (2010) Damascene process for controlled positioning of magnetic colloidal nanocrystals. Adv Mater 22:1364–1368

[21] Yang XM, Liu C, Ahner J, Yu J, Klemmer T et al (2004) Fabrication of FePt nanoparticles for self-organized magnetic array. J Vac Sci Technol B Microelectr Nanometer Struct 22:31–34

[22] Seo I, Kwon CW, Lee HH, Kim YS, Kim KB et al (2009) Completely filling anodic aluminum oxide with maghemite nanoparticles by dip coating and their magnetic properties. Electrochem Solid-State Lett 12:K59–K62

[23] Galloway JM, Bramble JP, Rawlings AE, Burnell G, Evans SD et al (2012) Biotemplated magnetic nanoparticle arrays. Small 8:204–208

[24] Galloway JM, Bramble JP, Rawlings AE, Burnell G, Evans SD et al (2012) Nanomagnetic arrays formed with the biomineralization protein Mms6. J Nano Res 17:127

[25] Bird SM, El-Zubir O, Rawlings AE, Leggett GJ, Staniland SS (2016) A novel design strategy for nanoparticles on nanopatterns: interferometric lithographic patterning of Mms6 biotemplated magnetic nanoparticles. J Mater Chem C Mater Opt Electr Dev 4:3948–3955

[26] Bird SM, Rawlings AE, Galloway JM, Staniland SS (2016) Using a biomimetic membrane surface experiment to investigate the activity of the magnetite biomineralisation protein Mms6††Electronic supplementary information (ESI) available: Including Mms6 protein and peptide sequences, additional QCM-D and SEM dat. RSC Adv 6:7356–7363

[27] Liu N, Liang W, Mai JD, Liu L, Lee GB et al (2014) Rapid fabrication of nanomaterial electrodes using digitally controlled electrokinetics. IEEE Trans Nanotechnol 13:245–253

[28] Wei F, Lee GB, Yu H, Lai HSS, Liu L et al (2015) Optically-controlled digital electrodeposition of thin-film metals for fabrication of nano-devices. Opt Mater Express 5:838–848

[29] Li P, Liu N, Yu H, Wang F, Liu L et al (2016) Silver nanostructures synthesis via optically induced electrochemical deposition. Sci Rep 6:28035

[30] Wang D, Wang Z, Zhang Z, Yue Y, Li D et al (2013) Effects of polarization on four-beam laser interference lithography. Appl Phys Lett 102:081903

[31] Zhao L, Wang Z, Zhang J, Cao L, Li L et al (2015) Antireflection silicon structures with hydrophobic property fabricated by three-beam laser interference. Appl Surf Sci 346:574–579

[32] Li L, Wang Z, Li W, Peng K, Zhang Z et al (2015) Fabrication of Pt nanowires with a diffraction-unlimited feature size by high-threshold lithography. Appl Phys Lett 107:133104

[33] Zhou Z, Song Z, Li L, Zhang J, Wang Z (2015) Fabrication of periodic variable-sized Pt nanoparticles via laser interference patterning. Appl Surf Sci 335:65–70

[34] Ghandoor HE, Zidan HM, Khalil MMH, Ismail MIM (2012) Synthesis and some physical properties of magnetite (Fe_3O_4) nanoparticles. Int J Electrochem Sci 7:5734–5745

[35] Mills P, Sullivan JL (2000) A study of the core level electrons in iron and its three oxides by means of X-ray photoelectron spectroscopy. J Phys D Appl Phys 16:723–732

[36] Pamela C, Richard A, Denise R (2005) Lippincotts illustrated reviews biochemistry. Lippincott Williams and Wilkins, Philadelphia

[37] Temesghen W, Sherwood P (2002) Analytical utility of valence band X-ray photoelectron spectroscopy of iron and its oxides, with spectral interpretation by cluster and band structure calculations. Anal Bioanal Chem 373:601–608

[38] Gamburg YD, Zangari G (2011) The structure of the metal-solution interface. Theory and practice of metal electrodeposition. Springer, Berlin, pp 27–51

[39] Morgan H, Green NG (2003) AC electrokinetics. Research Studies Press, Philadelphia

[40] Fang Y, Liu Z (2010) Electrochemical reactions at the electrode/solution interface: theory and applications to water electrolysis and oxygen reduction. Sci China Chem 53:543–552

[41] Trasatti S (1983) Physical, chemical and structural aspects of the electrode/solution interface. Electrochim Acta 28:1083–1093

[42] Moddel G, Anderson DA, Paul W (1980) Derivation of the low-energy optical-absorption spectra of a-Si: H from photoconductivity. Phys Rev B 22:1918–1925

[43] Hashimoto T, Yamada T, Yoko T (1996) Third-order nonlinear optical properties of sol–gel derived α-Fe_2O_3, γ-Fe_2O_3, and Fe_3O_4 thin films. J Appl Phys 80:3184–3190

Journal : **10853**
Article : **1788**

Springer
the language of science

Author Query Form

Please ensure you fill out your response to the queries raised below and return this form along with your corrections

Author Proof

Dear Author

During the process of typesetting your article, the following queries have arisen. Please check your typeset proof carefully against the queries listed below and mark the necessary changes either directly on the proof/online grid or in the 'Author's response' area provided below

Query	Details Required	Author's Response
AQ1	Please check the edit made in the article title.	
AQ2	Please confirm the section headings are correctly identified.	
AQ3	Please provide end page range for the references [2, 4, 6, 7, 9, 19, 24, 26, 30, 32].	